Scientia Iranica A (2019) 26(4), 2176–2186

Sharif University of Technology
Scientia Iranica
Transactions A: Civil Engineering
http://scientiairanica.sharif.edu

Invited Paper

A new method of determining the collapse capacity and risk of RC structures incorporating near-fault pulse period effect by considering confinement ratio

H. Shanehsazzadeh and M. Tehranizadeh*

Faculty of Civil Engineering, Amirkabir University of Technology, 424, Hafez Ave., Tehran, Iran.

Received 17 February 2019; accepted 28 May 2019

KEYWORDS
Collapse probability;
Risk;
Near-fault;
Pulse period;
Confinement ratio;
Backbone behavior;
Axial load ratio.

Abstract. Collapse capacity is one of the fundamental factors in evaluating collapse risk in the performance-based design engineering field. Calculation of this parameter has been time-consuming during the past decade. This issue has prevented engineers from determining this parameter in a prevalent and practical way. Furthermore, defining of this value has been found more challenging in a near-source region due to special characteristics of its pulse-like records, which make the collapse capacity more dependent on period ratio, T/Tp. In this study, a method was proposed to obtain collapse capacity of Reinforced Concrete (RC) structures considering two main variables affecting the behavior of columns, namely axial load ratio and confinement ratio. The mentioned method eschewed the intensive computational challenges of incremental dynamic analyses to find collapse probability. By the proposed approach, the pulse period impact was incorporated into collapse risk using probabilistic equations. After the role of axial load ratio was illustrated, the resulting collapse probability distributions and the corresponding risk values were obtained for a near-fault site. The results explained that as the confinement ratio descended, the collapse capacity with near-fault pulse effect was decreased and the risk values were raised, consequently. In addition, the results were found in compliance with ASCE acceptable risk value.

1. Introduction

Development of risk-based decision, which has drawn the interest of engineers, urban planners, insurance underwriters, and regulatory authorities, is reaching a state of maturity [1]. Consequently, in performance-based engineering, one of the crucial issues discussed heatedly is evaluation of collapse risk and building codes are intended to meet the considerations of this issue [2-4].

Collapse risk has two main components, namely hazard of the site and collapse capacity of the structure. Discussions of different approaches to collapse risk calculation show that the risk integral derivative of the fragility curve is more accurate than that derivative of the hazard curve [5]. The hazard curve derived by probabilistic seismic hazard analysis and collapse capacity of structures defined by IDA (Incremental Dynamic Analysis) calculations have been coupled by the risk integral in order to determine the risk value [2].

In all the above-mentioned researches, effects of near-fault sites were not considered. In fact, near-

*. *Corresponding author. Tel.: +98 21 6454 3030*
E-mail addresses: homa_shanehsaz@yahoo.com (H. Shanehsazzadeh); dtehz@yahoo.com (M. Tehranizadeh)

doi: 10.24200/sci.2019.21438

fault pulse-like events have distinctive features due to the forward directivity phenomenon, which makes them significant and distinguishable from ordinary ground motions. Hence, they have drawn attention of the engineers in this paradigm. The characteristics of this type of motions are explained concisely in terms of a single double-sided, early-arriving pulse with most of the energy of the time history record [6,7]. Since ground motions in near-fault sites have some specific features that differentiate them from ordinary ground motion records, as stated above, specific investigations into their effects on structures seem to be necessary [8,9]. Probabilistic seismic hazard analysis has been improved for near-fault motion, individually [10,11]. Valuable researches dealt with the fragility curves and collapse capacity distributions of various types of structures without considering near-faults impacts [12,13], although some others addressed near-fault collapse capacity by using pulse-like records for applying IDA to buildings. The results explained considerable reduction in near-fault collapse capacity of structures in addition to the undeniable effect of ductility and period ratio, defined as the ratio of fundamental period of structure to the pulse period, T/T_P [14,15].

Structure ductility plays an important role in meeting the collapse capacity requirements, which play a key role in modern building codes [12,14]. If the ductility of a structure is high enough, it helps the most to get the collapse capacity curve, which is required in the given site. Therefore, adapting ductility in design is very effective to obtain the required collapse capacity [13,15]. In fact, it is necessary to define some basic design properties such as confinement ratio for a structure supposed to be built. Confinement ratio and axial load ratio have a major role in ductility of a structure, which is basically provided by the backbone behavior [16]. In case of being able to adjust backbone behavior parameters, we can expect the required ductility. In order to achieve this goal, in this paper, the association between two factors in designing and adjusting backbone behavior has been considered. The two factors are, ρ_{sh}, which is confinement ratio explained as transverse reinforcement ratio, and ν, which is axial load ratio and has an important effect on the amount of collapse capacity. These two factors together affect the backbone behavior parameters sensibly and comprehensively.

In the present study, the impact of each parameter on collapse capacity in near-source zone has been investigated. Afterwards, the near-fault pulse effect is incorporated with the help of probability relationships in order to find the risk value. In this method, the pulse rule is directly implemented in risk integral by the pulse probability term derived from hazard desegregation. One of the advantages of this approach is that the determined risk value includes pulse period impact and invariability for a considered site. Moreover, collapse capacity curves will be obtained incorporating the near-fault pulse period effect and compared with collapse capacity curves derived from ASCE7-16 as well as the risk values. The highest amount of risk value determined by the proposed approach belongs to the high axial load category with confinement ratio of 0.002. It is the only value exceeding the required risk of ASCE, which implies that the confinement ratio does not meet the required collapse risk value and the structure is not conservative from the risk aspect. However, other design criteria are acceptable. Also, other investigated categories comply with the acceptable risk value of the building code. It shows that the design criteria are sufficient to satisfy the risk condition.

2. Methodology and assumptions

In performance-based design, one of the most fundamental issues is collapse capacity. It plays an ascertainable role in determining the collapse risk, which has been the key parameter of design in recent provisions [3]. Therefore, it is essential to assess collapse capacity and consequently collapse risk, especially the near-fault ones. For this purpose, period ratio is one of the crucial factors selected to be investigated with regard to its impacts on collapse capacity in near-fault zones. The ratio of the fundamental period of the structure to the pulse period presents the period ratio T/T_p [12].

The efficient model presented by Baltzopoulos et al. [17] is applied in order to calculate collapse capacity ratio. Collapse capacity ratio is described as the ratio of the spectral acceleration causing collapse to the yield spectrum acceleration of the structure in fundamental vibration period. In that model, the static pushover curve is needed for a given structure. The fundamental vibration period is assumed to be 1 sec in this study, although any other value can be assigned. Assuming 1 sec is efficient, since in building codes, it is addressed as a main parameter to define design spectrum and follow other design criteria [3]. Also, 5% damping is considered as suggested widely in the literature. When we use collapse capacity ratio instead of collapse capacity, it can enhance our understanding of the general capacity of a structure in collapse state. Furthermore, as we want to delve deeper into ductility impact on collapse capacity continuously and generally, the tri-linear backbone behavior curve is applied with a variety of ductility behaviors. Hence, we need backbone behavior curves with variable ductility. Figure 1 depicts different definitions of ductility in the presented tri-linear backbone. In this figure, μ_c is ductility at capping point and μ_{end} is obtained by

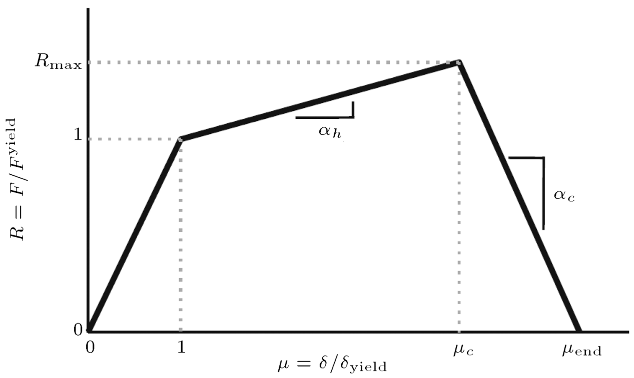

Figure 1. Backbone behavior curve and its three main parameters [17].

Eq. (1) [17]:

$$\mu_{end} = \mu_c + (1 + \mu_c.\alpha_h - \alpha_h)/|\alpha_c|. \quad (1)$$

It is logical to control all parts of the curve by only three parameters of μ_c, α_h, and α_c. Total behavior curve is defined as a function of integrated results from the three mentioned parameters (Figure 1). Consequently, it is needed to have a unique variable which controls all backbone behavior elements. Then, it is possible to comprehensively and reasonably judge the behavior of the collapse capacity of the systems. This research suggests the key parameter of confinement ratio, which is described as $\rho_{sh} = \frac{A_{sh}}{sb}$, where A_{sh}, s, and b are total cross-sectional area of transverse reinforcement; spacing of transverse reinforcement, which is measured along the height of the column; and the width of the column, which is measured perpendicular to transverse load, respectively. Confinement ratio is the adjusting parameter required and ductility behavior can directly depend on it.

We use Haselton et al. relationships for providing the required connection relationships between confinement ratio and backbone behavior properties [16]. They are brought as Eqs. (2)-(5):

$$M/My = (1.25)(0.89)^{\nu}(0.91)^{0.01f'_c}, \quad (2)$$

$$\nu = P/A_g.f'_c,$$

$$\theta_{pc}= (0.76)(0.031)^{\nu}(0.02 + 40\rho_{sh})^{1.02} \leq 0.10, \quad (3)$$

$$\theta_{cap,tot}= (0.14)(0.19)^{\nu}(0.02 + 40\rho_{sh})^{0.54}(0.62)^{0.01f'_c}$$

$$\text{(without bond-slip)}, \quad (4)$$

$$\theta_y=\varphi_y.L_s/3 + 0.00275 \quad \text{(without bond-slip)}$$

$$\varphi_y= 2.12\varepsilon_y/h. \quad (5)$$

The mentioned parameters are shown in Figure 2. In this way, it will be possible to provide different

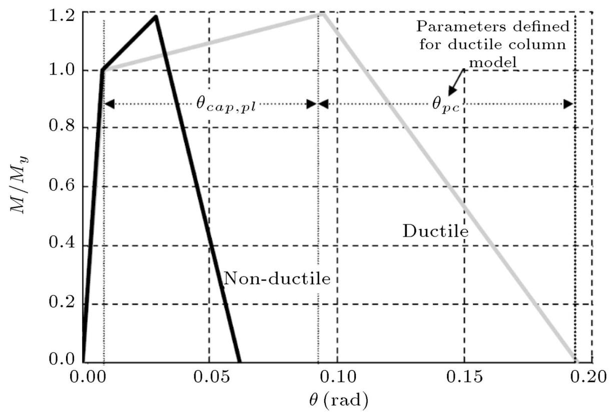

Figure 2. Example of backbone behavior defined by related parameters of Haselton relationships [16].

reasonable backbone behavior curves for analysis and obtain the outcome looked for. It is worth stating that an average amount of $M/M_y = 1.13$ is suggested by Haselton for cantilever columns due to the fact that this ratio will not change significantly by various values of axial load ratio and transverse steel ratio [16].

As it can be understood from Eqs. (2) to (5), backbone behavior parameters are mainly controlled by confinement ratio factor. However, axial load ratio is also noticeable. Therefore, calculations are divided into two groups: low axial load ratio, 0.1, and high axial load ratio, 0.24. These values are commonly used [18]. Consequently, the results will be provided for these two groups, separately. Different backbone behavior curves are obtained by the above-mentioned quantities in 4 practically prevalent confinement ratio levels. Afterwards, collapse capacity will be calculated with the help of Baltzopoulos et al. model [17] for different period ratios as well.

As defined previously, period ratio is another known effective parameter in pulse conditions. Various methods are employed for finding the amount of pulse period such as the maximum velocity spectrum and Baker method [6,11]. In Baltzopoulos et al.'s procedure [17], Baker's method has been considered. We want to explore its role in collapse capacity with confinement ratio, as a behavior or ductility representative parameter, simultaneously. Moreover, in order to incorporate the pulse period effect into collapse capacity and risk evaluation, probabilistic estimations and pulse period contributions in a near-fault site are employed. The respective relationships will be explained later and, eventually, the results will be discussed.

3. An insight into period ratio impact on collapse capacity in different ductility behaviors

The considered system described previously is analyzed with different period ratios. The tri-linear backbone

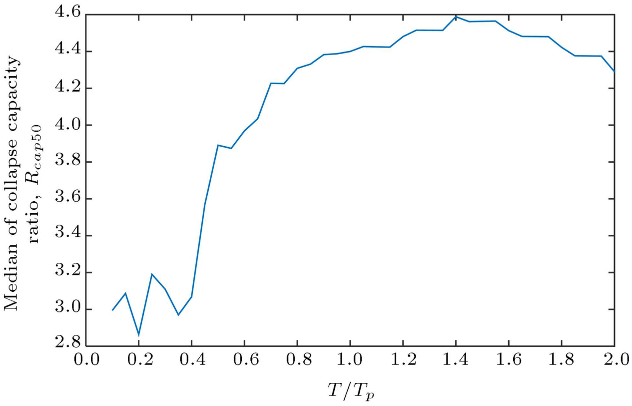

Figure 3. An example of collapse capacity ratios values for various period ratio ($\mu_c = 2$, $\alpha_{\text{soft}} = 0.2$, $\alpha_{\text{hard}} = 0.13$).

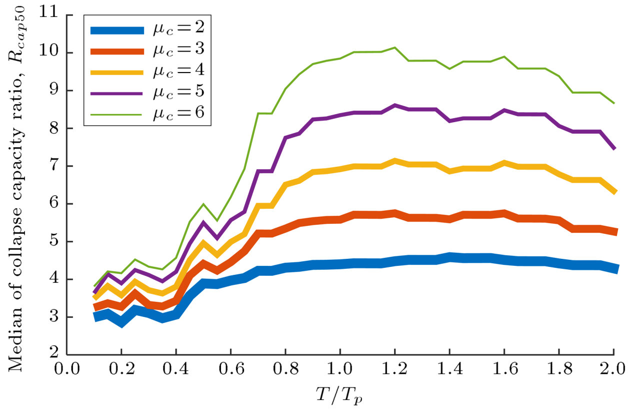

Figure 4. Collapse capacity values for various period ratios and ductility quantities.

behavior is obtained by values of $\mu_c = 2$, $\alpha_{\text{soft}} = 0.2$, and $M/M_y = 1.13$. The amount of α_{hard} is calculated by Eq. (6):

$$\alpha_{\text{hard}} = (Mc/My - 1)/(\mu_c - 1). \tag{6}$$

The median values of collapse capacity ratio, Rcap50, were determined for different amounts of period ratio. Figure 3 depicts the effect of period ratio on collapse capacity in pulse condition for the mentioned case. As it can be seen, collapse capacity increases with period ratio T/T_p from about 0.4 to 1.4, consistently. After this range, a slight reduction in collapse capacity is observed. On the other hand, before the period ratio of 0.4, a consistent trend is not recognized. This general trend implies that for pulse periods less than the effective period of the structure, which is higher than the fundamental period, the collapse occurs at lower values and therefore, at earlier times, while in pulse periods close to or higher than the structure effective period, the collapse capacity is larger and the probability of collapse drops dramatically.

It is worth mentioning that $0.1 < T/T_p < 2$ is selected as the period ratio range, since before and after this span, results are the same as those at thresholds [17]. The step for increase in period ratio is considered 0.05; thus, 40 points are applied to this part.

For a broader insight into the impact of period ratio on collapse capacity in different amounts of ductility, the results in Figure 4 can be perused. The general trend of rising uniformly and then, negligible reduction in collapse capacity ratio can be seen by the increase in period ratio of curves. Furthermore, with increase in the amount of ductility, μ_c, the augmentation of the collapse capacity ratio is observed. In fact, when the structure is more ductile, collapse capacity is higher; therefore, collapse occurs later than in less ductile structures. It implies that collapse probability is attenuated by increasing the ductility.

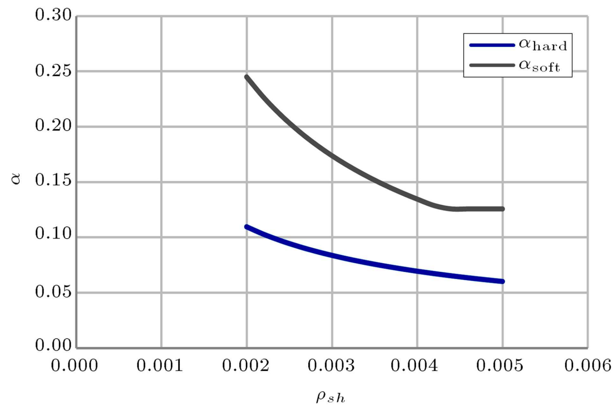

Figure 5. Variation of α_{hard} and α_{soft} with confinement ratio ($\nu = 0.1$).

4. Using confinement ratio as a main controller of tri-linear backbone behavior to obtain collapse capacity ratio

In the previous section, the average $M/M_y = 1.13$ and $\alpha_{\text{soft}} = 0.2$ were considered with different ductility values of μ_c for analysis. Nonetheless, we want to deal with a more comprehensive condition of behavior. Changing μ_c, α_{soft}, and α_{hard} individually is far from reality, because in real behavior, all these three parameters change together and they integrally define a particular behavior. Therefore, it is decided to consider confinement ratio as the dominant parameter for determining μ_c, α_{soft}, and α_{hard}. The assessment of the dependence of these three parameters on confinement ratio is presented in Figures 5 and 6 with the help of Eqs. (2) to (5). The results are calculated for a 3 m high concrete cantilever column with $h = b = 55$ cm as an assumed system with $f'_c = 30$ MPa. Figures 5 and 6 show that as confinement ratio rises, hardening and softening slops decrease and μ_c grows, which leads to a more ductile behavior.

In the following, the collapse capacity ratio is determined by considering period ratio and confinement

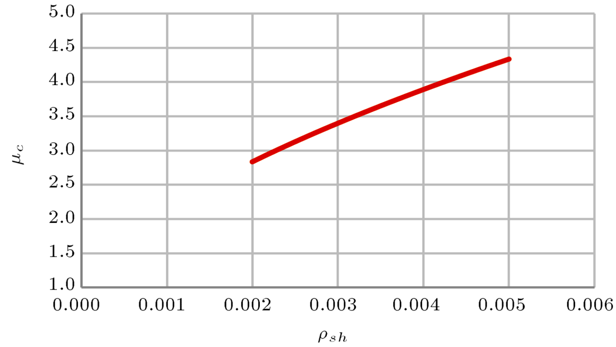

Figure 6. Variation of μ_c with confinement ratio ($\nu = 0.1$).

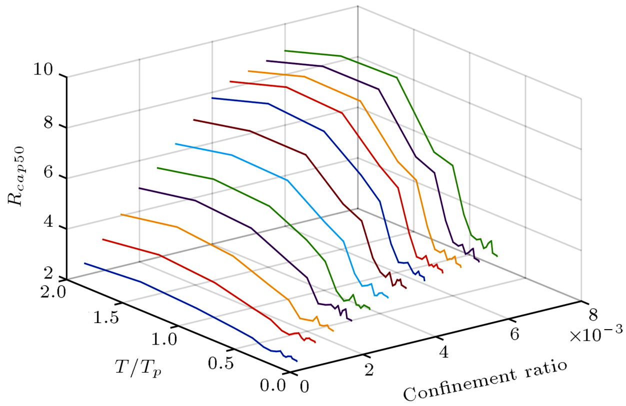

Figure 7. Collapse capacity ratio as a function of confinement ratio and period ratio for low axial load ratio.

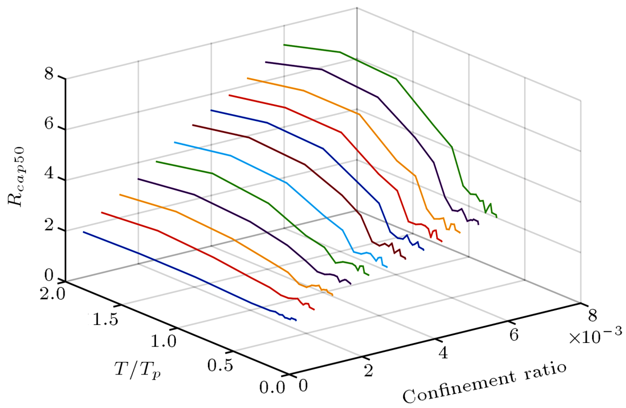

Figure 8. Collapse capacity ratio as a function of confinement ratio and period ratio for high axial load ratio.

ratio variable. Figures 7 and 8 illustrate the quantities of the collapse capacity ratio in pulse condition as a function of period ratio and confinement ratio for the mentioned structure in two categories of low and high axial load ratios. In both figures, we perceive the same raising tendency at first and then, nearly uniform trend of collapse capacity by growing period ratio in different levels of confinement ratio, although we should notice the dissimilar values of collapse capacities at maximum

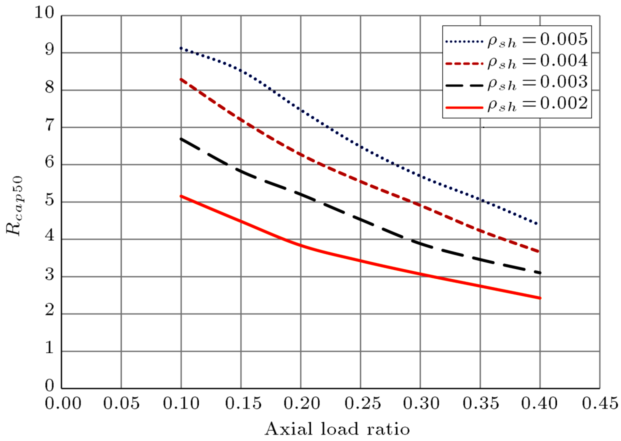

Figure 9. Collapse capacity ratio variation with axial load ratio for different confinement ratio levels.

levels for the diagrams of low and high axial load ratios. The pattern of changes with period ratio is similar to what mentioned for each μ_c, since confinement ratio has a direct effect on μ_c. Hence, the interpretation of the observed varieties is akin to that of Figures 3 and 4. As we expected, the amounts of collapse capacity ratio are less for high than for low axial load ratio. Moreover, by considering constant period ratio, decreasing the confinement ratio leads to higher collapse capacity ratio due to the lower ductility.

5. Reconsideration of the influence of axial load ratio on collapse capacity

In this section, we delve deeper into the impact of axial load ratio on collapse capacity. Therefore, for different values of axial load ratio, backbone behavior parameters are calculated as explained before and analysis is conducted to find the amounts of collapse capacity ratio with different values of confinement ratio. It is carried out for different period ratios, but presented here for $T/T_p = 1$ for the sake of brevity. The same trend can be observed for other values of T/T_p. As anticipated, the diagram in Figure 9 indicates that the collapse capacity ratio is reduced dramatically by enhancing axial load ratio at different confinement ratio levels, because higher axial load ratio increases the collapse probability.

6. Collapse capacity curve for near-fault site including pulse period effect at different confinement ratios

In this section, we will follow the procedure of developing the collapse capacity curve for a given confinement ratio by including the pulse period effect.

The median of collapse capacity ratio can be considered as a function of pulse period and confinement ratio, as it was explained in previous sections. Due to

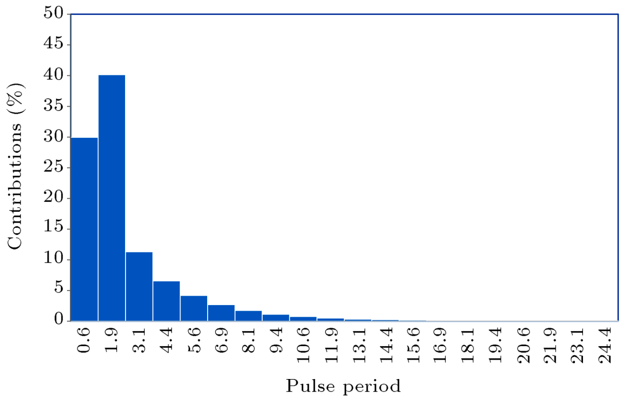

Figure 10. Probability distribution function of pulse period for Tabriz near-fault site [10].

variability of pulse period values, it is generally possible for T_p to occur at all considered values. Hence, in near-fault condition, the probability distribution of collapse capacity should incorporate pulse period variability. Then, the expectation of collapse capacity ratio for each confinement ratio can approximately be expressed by Eq. (7) [19] in pulse condition:

$$E[\ln R_{\rho_{sh}}|\text{pulse}] \approx \sum_i \ln R_{50\%,\rho_{sh}}(T_p).P_{t_{pi}}, \qquad (7)$$

where, given T_p, $R_{50\%,\rho_{sh}}(T_p)$ is the median of collapse capacity ratio for each confinement ratio and $P_{t_{pi}}$ is probability of pulse period expressed as $P[T_p = t_{pi}|Sa(1s)]$. An example of this distribution function for the Tabriz near-fault site has been investigated by Yousefi and Taghikhany, which is depicted in Figure 10 [10]. It is clear that, generally, as pulse period increases, the probability of pulse occurrence, which is mentioned by the contribution term in Figure 10, is reduced. Nonetheless, the rise of contribution in 1.9 sec can be seen at the beginning limit. It is worth stating that this illustration is calculated for a given spectral acceleration of the mentioned region of 0.37 g (475 yrs return period) at the fundamental vibration period of 1 sec, as considered in the previous sections. The mentioned spectral acceleration will be used for inverting the resulting collapse capacity curve from normalized variable $Sa_{\text{collapse}}/Sa_{\text{yield}}$ to Sa_{collapse}.

According to the Iranian code of practice for seismic resistant design of buildings (Standard no. 2800) [20], for the stated site, we have Type-I soil category, which belongs to the high seismic region. Since design-based acceleration is calculated considering near-fault effects, we do not need to employ the near-fault coefficient here. Consequently, AB, which corresponds to S_{DS} from ASCE7-16, equals 0.37. Assuming the moderate importance group for the structure, like residential buildings, the importance factor I_e equals 1. Moreover, as we have a cantilever system, response modification coefficient is determined as $R_e = 1.5$. Seismic response coefficient, C_s, and effective seismic weight, W, are used for calculating the base shear parameter, V in the following equations:

$$C_s = S_{DS}.I_e/R_e = 0.247, \qquad V = C_sW.$$

As stated by FEMAP695 [4], based on the assumption that 100% of the effective seismic weight of the structure, W, participates in the fundamental mode in the period, V is consistent with the yield base shear in static pushover. Therefore, C_s is considered as Sa_{yield}. Thus, the calculated Sa_{yield} will change the collapse capacity ratio, R, to Sa_{collapse} after we prepare the collapse capacity ratio probability function.

Another coefficient that we use to obtain the probability distribution function is variance. Since collapse capacity function is assumed to follow lognormal distribution in the literature [2,19], by the use of median and variance of this distribution, we can define the distribution curve. Conditional variance is defined by Eqs. (8) and (9) [19]:

$$Var[\ln R_{\rho_{sh}}|\text{pulse}] \simeq \sum_i Var[\ln R_{\rho_{sh}}|T_p].P_{t_{pi}} + \sum_i (E[\ln R_{\rho_{sh}}|\text{pulse}] - \ln R_{50\%,\rho_{sh}}(t_{pi}))^2.P_{t_{pi}}, \qquad (8)$$

$$Var[\ln R_{\rho_{sh}}|T_p] = [\ln R_{84\%,\rho_{sh}}(t_{pi}) - \ln R_{16\%,\rho_{sh}}(t_{pi})]^2/4. \qquad (9)$$

FEMAP695 [4] suggested the values for record to record variability or standard deviation, β_{RTR}. They are compared with our results in Table 1 considering pulse effect. β_{RTR} is obtained by Eq. (10) [3] for

Table 1. Values of record to record varibility, β_{RTR}.

	Low axial load ratio		High axial load ratio	
ρ_{sh}	Standard deviation	FEMA	Standard deviation	FEMA
0.002	0.33	0.38	0.27	0.32
0.003	0.38	0.40	0.30	0.37
0.004	0.40	0.40	0.34	0.40
0.005	0.42	0.40	0.41	0.40

different amounts of ductility corresponding to the amounts of μ_{end}. The definition for ductility variable in FEMAP695 is the ratio of displacement corresponding to 80% $V_{\max}$ in pushover diagram to the yield displacement, which leads to an approximate estimation of μ_{end}. Thus, ductility variable is found out by the related μ_{end} for each ρ_{sh}. Although the values of β_{RTR} are suggested for ordinary condition by FEMAP695, not near-fault sites, a rough compliance of quantities can be observed in Table 1. It is worth mentioning that different FEMA values in different columns for low and high axial load ratios were derived with different values of μ_{end}.

$$0.2 \leq \beta_{RTR} = 0.1 + 0.1\mu \leq 0.4. \tag{10}$$

$R_{50\%,\rho_{sh}}(T_p)$, defined as median value of collapse capacity ratio for each ρ_{sh}, given T_p, is calculated and presented in Figures 7 and 8 for low and high axial load ratios, respectively. We intend to obtain the median collapse capacity probability for the exampled near-fault site incorporating pulse period impact. Thus, we utilize $R_{50\%,\rho_{sh}}(T_p)$ and probability of pulse period $P_{t_{pi}}$ as stated in Eq. (7). $P_{t_{pi}}$ is a separate probability distribution for each spectral acceleration multiplied by $R_{50\%,\rho_{sh}}(T_p)$ corresponding to the related Sa_{collapse}. The obtained result is presented in Table 2 for two groups of axial load ratios and different confinement ratio levels.

The results of the mentioned calculations are shown in Figures 11-14 for both probability density distribution and cumulative distribution functions. Although the values in Table 2 are used to achieve probability functions, the appropriate changes of variables from R to Sa_{collapse} have been considered by Sa_{yield}, as explained previously. The calculated results are shown in Table 3 for low axial load ratio cases. Capacity curves for pulse condition incorporating pulse period impact are illustrated as probability density functions in Figure 11 and cumulative distribution functions of collapse capacity in Figure 12 for low axial load ratio and distinctive confinement ratio levels. Figures 13 and 14 indicate results akin to those in Figures 11 and 12, but for high axial load ratios.

The increase in median of collapse capacity with heightening confinement ratio is observable in Figures 11 and 13. It can be perceived from these two diagrams that the collapse capacity is lower in high axial load ratio (Figure 13) than in low axial load ratio (Figure 11) for the same considered confinement ratio, as expected. Figures 12 and 14 demonstrate

Table 3. Median values of Sa_{collapse} incorporating pulse period effect for low axial load ratio.

ρ_{sh}	E[R|pulse]	$Sa_{\text{collapse}} = R.Sa_{\text{yield}}$
0.002	5.16	1.27
0.003	6.69	1.65
0.004	8.28	2.05
0.005	9.12	2.25

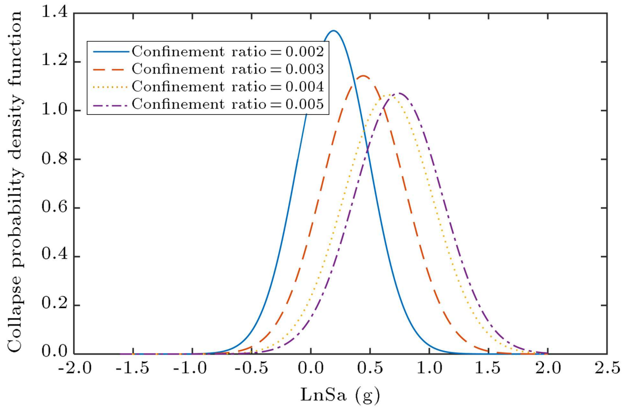

Figure 11. Collapse capacity curves including pulse period impact for low axial load ratio ($\nu = 0.1$).

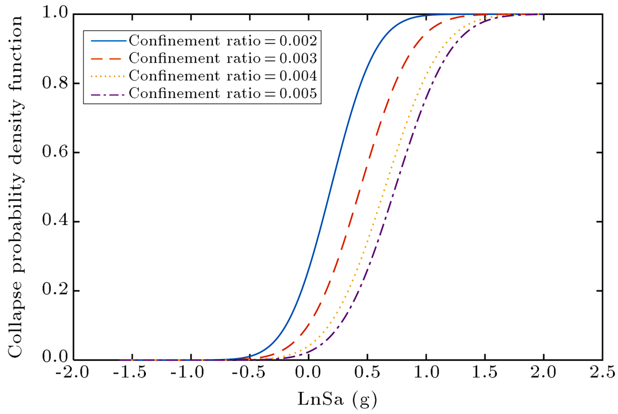

Figure 12. Cumulative collapse probability functions including pulse period impact for low axial load ratio ($\nu = 0.1$).

Table 2. Median and variance of natural logarithm of collapse capacity ratio for two groups of axial load ratios and different confinement ratios.

	LnR for low axial load ratio		LnR for high axial load ratio	
ρ_{sh}	Median	Variance	Median	Variance
0.002	1.64	0.11	1.25	0.07
0.003	1.90	0.14	1.54	0.09
0.004	2.11	0.16	1.74	0.12
0.005	2.21	0.18	2.07	0.17

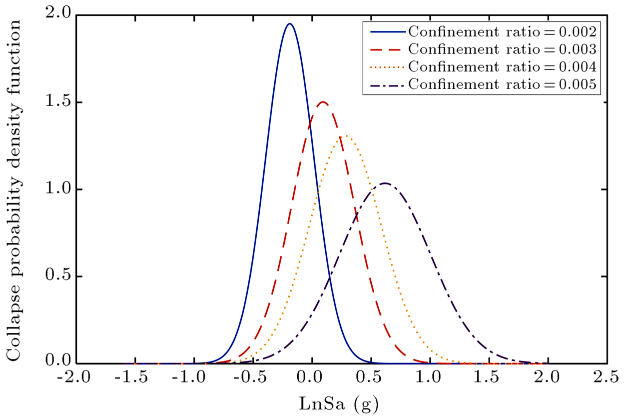

Figure 13. Collapse capacity curves including pulse period impact for high axial load ratio ($\nu = 0.24$).

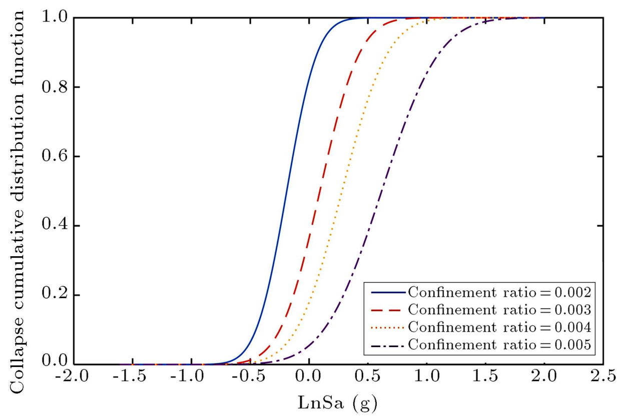

Figure 14. Cumulative collapse probability functions including pulse period impact for high axial load ratio ($\nu = 0.24$).

the stated issue for cumulative quantities. The growth of collapse capacity by enhancing confinement ratio is significant in both figures. The observed results show that when the axial load ratio is higher or confinement ratio is lower, the probability of collapse increases for the considered spectral acceleration.

In the following, comparison of the presented procedure with the results from ASCE7-16 is provided. S_{M1}, in ASCE, addresses spectral acceleration with 10% probability of collapse and total standard deviation of 0.6. Thus, by finding the amount of SM_1 for the considered location, we can obtain the related median of spectral acceleration of collapse capacity to compare with the results of the presented method. A location with the same seismological features has been selected. This location is considered as the corresponding site due to the same value of $S_{M1} = 0.37$ g in the ASCE map. Then, the median for log-normal distribution is calculated at 1.2 g, which is slightly lower than the median amount of Sa_{collapse} presented for confinement ratio of 0.002 in Table 3 for low axial load ratio.

It is worthy to note that the proposed method

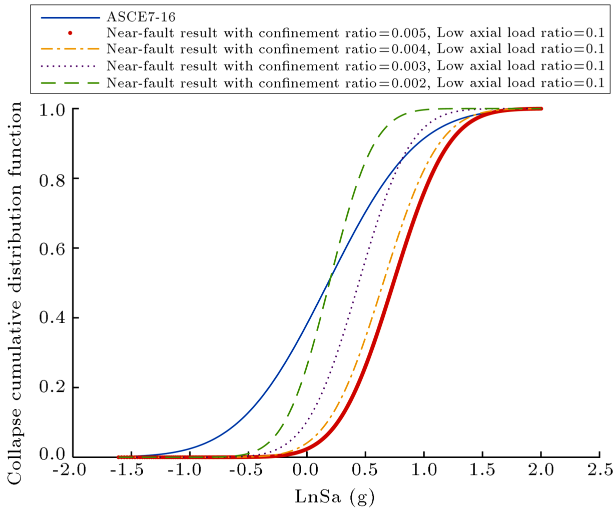

Figure 15. Collapse probability functions for near-fault incorporating pulse period and low axial load ratio in comparison with ASCE7-16.

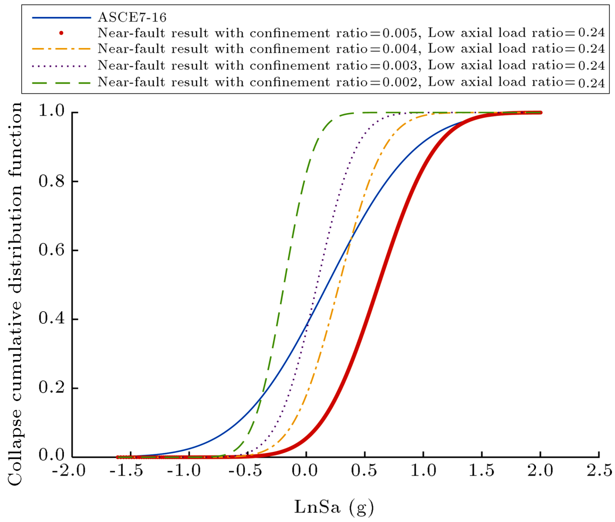

Figure 16. Collapse probability functions for near-fault incorporating pulse period and high axial load ratio in comparison with ASCE7-16.

incorporates pulse period effect and confinement ratio in near-fault region, which are not mentioned in the ASCE results. Moreover, in this method, record to record variability is included, while ASCE considers a constant value of 0.6 for total uncertainty [3]. The related collapse capacity diagram is obtained to compare with the presented method. The research results are superimposed on the corresponding curves of ASCE7-16 in Figures 15 and 16 for low and high axial load ratios, respectively.

In Figure 15, it is observable that the median Sa of collapse derived from ASCE7-16 does not exceed the median value in the diagrams of the near-fault results incorporating pulse period effect. At 0.002 confinement ratio level in the case of low axial load ratio, for spectral accelerations lower than 1.23 g corresponding to 52% collapse probability, ASCE7-16 shows lower collapse Sa with higher probability. For other confinement ratios, nearly all of the capacity curves are under what is shown by ASCE7-16. The figure implies that the results present lower collapse probability along with higher collapse capacity than the curve by ASCE does, demonstrating that the building code is conservative from this aspect.

Figure 16 shows that at confinement ratio of 0.005, for nearly all collapse probabilities, the amounts of Sa demanded by ASCE7-16 are lower than the collapse value of Sa found, while at confinement ratio of 0.004, for the probability of 0.64, the corresponding values of ASCE exceed the capacity. This probability and the corresponding spectral acceleration are about 0.17 and 0.68 g, respectively, for confinement ratio of 0.002. In fact, for probabilities less than 0.17, the capacity needed by ASCE is lower than the capacity depicted for this confinement ratio. From the viewpoint of design, a low range of probability, about 0.1, is concerned, as it was mentioned before [3]. Therefore, it can be concluded that Figure 16 illustrates proper consistency of the cumulative distribution function of collapse capacity from ASCE7-16 with the near-fault distribution function computed with pulse period impact.

Since ASCE curve has been proven to be in complete compliance with the research results, as depicted, it can be concluded that if a structure is designed based on ASCE7-16, it can meet the collapse capacity requirements, because it shows higher collapse Sa than what the building code requires. However, it is suggested, for more comprehensive judgment, that the risk of near-fault collapse with pulse ratio impact be obtained in order to incorporate the variability of collapse spectral acceleration.

7. Near-fault risk analysis results with period impact

In this section, collapse risk for the mentioned structures is calculated. Ordinary estimation of collapse risk (in far-field sites) uses risk integral. In fact, risk integral includes spectral acceleration uncertainty as shown in the following equation:

$$Risk = \int_{Sa} f(col|Sa)H(Sa)\,dSa. \tag{11}$$

This equation has two basic parts: 1) the conditional collapse probability, which is the probability of collapse for each given spectral acceleration; 2) hazard curve, which gives the occurrence probability of spectral accelerations. By using the total probability theory, the collapse probability (independent from spectral acceleration) is obtained, which is called risk.

Table 4. Annual risk of collapse.

	Low axial load ratio			
Confinement ratio	0.002	0.003	0.004	0.005
Risk ($\times 10^{-4}$)	0.6	0.2	0.1	0.1
	High axial load ratio			
Confinement ratio	0.002	0.003	0.004	0.005
Risk ($\times 10^{-4}$)	2.6	0.8	0.4	0.1

In the previous researches [14,15], near-fault collapse risk was defined similarly to far-field, but by employing near-fault hazard curve $H^*(Sa)$ or incremental dynamic analysis by near-fault records. In this study, it is intended to incorporate the pulse period effect in the near-fault collapse risk estimation. On the other hand, the near-fault collapse capacity of structures is a function of the pulse period as well as spectral acceleration and can be explained as a two-variable conditional probability function. Furthermore, the probability of pulse period plays an important role in collapse risk, because in structures with fundamental period close to the pulse period, the collapse probability is higher. In fact, in near-fault sites, the probability of pulse period is related to acceleration and they are not independent. Therefore, the result derived in the previous section is multiplied by the near-fault hazard curve in order to determine the near-fault collapse risk by considering pulse period impact.

In the following, collapse risk is defined by incorporating pulse period effect and the results are provided in Table 4. This table shows higher collapse risk for lower confinement ratios. Moreover, collapse risk for low axial load ratios has lower values than for high axial load quantities. The annual uniform risk considered by ASCE7-16 is 0.0002 and all amounts of risk in Table 4 are acceptably lower than this limit. This implies the consistency of the presented procedure with the building code from the aspect of risk.

8. Conclusion

The present study investigated the pulse period impact on collapse capacity for different ductility behaviors defined by the fundamental coefficient of confinement ratio. The proposed method utilized Haselton relationships and the model presented by Baltzopoulos et al. to obtain reasonable ductility behaviors and analyze related systems, respectively, in order to find their collapse capacities. Moreover, an insight into the axial load ratio effects on collapse capacity was presented. Since the high axial load ratio increased the collapse probability, collapse capacity ratio dropped dramatically by increase in axial load ratio at different confinement ratio levels. Due to the significant role of axial load ratio in ductility behavior and, subsequently, in collapse capacity, analyses were carried on for two categories of low and high axial load ratios and the results were presented for both cases. In each category, the rise of collapse capacity ratio by period ratio was observed and it was observed that its rate grew when confinement ratio became larger. By means of probabilistic equations mentioned in this paper, the pulse period effect was incorporated in risk analysis. Finally, the results illustrated a good compliance with collapse capacity diagram derived from ASCE7-16. Besides, they proved the ASCE to be in a conservative state in comparison with the developed collapse capacity curves obtained by the new method. In addition, as the confinement ratio decreased, the collapse capacity with near-fault pulse effect was attenuated. The presented procedure can be applied to a wide variety of near-fault structures for incorporating pulse period impact in the expeditious approach. Furthermore, it can be employed straightforwardly in near-fault risk assessments. From the aspect of risk values, the building code limitation was also found conservative in comparison with quantities for near-fault analysis incorporating pulse effect in most of the confinement ratios.

Acknowledgement

The authors appreciate the supports of Georgios Baltzopoulos and Bruce R. Ellingwood, who provided invaluable clarifying information on the probability of collapse, specially about the MCE parameter in ASCE.

Nomenclature

M	Maximum moment capacity
M_y	Yield moment capacity
h	Height of column, measured parallel to transverse load (mm)
b	Width of column, measured perpendicular to transverse load (mm)
f'_c	Standard concrete compressive strength (MPa)
A_g	Gross cross section of column (bh) (mm^2)
P	Axial load (kN)
ν	Axial load ratio
ρ_{sh}	Transverse steel ratio
θ_{pc}	Post-capping plastic rotation capacity, from the cap to point of zero strength (rad)
$\theta_{cap,tot}$	Total (sum of elastic and plastic) chord rotation at capping (rad)
θ_y, L_s, φ_y, ε_y	Chord rotation at yielding, shear span (distance between column end and point of inflection) (mm), yield curvature, and yield strain of longitudinal reinforcement, respectively

References

1. Ellingwood, B.R. and Wen, Y. "Risk-benefit-based design decisions for low-probability/high consequence earthquake events in Mid-America", *Prog. Struct. Engng Mater*, **7**, pp. 56-70 (2005). DOI:10.1002/pse.191
2. Luco, N., Ellingwood, B.R., Hamburger, R.O., Hooper, J.D., Kimball, J. K., and Kircher, C.A., "Risk-targeted versus current seismic design maps for the conterminous United States", SEAOC, Convention Proceedings (2007).
3. ASCE "Minimum design loads for buildings and other structures", *ASCE/SEI 7-16*, American Society of Civil Engineers: Reston, Virginia (2016).
4. Applied Technology Council "Quantification of building seismic performance factors (FEMA P695)", *NEHRP Recomended Provisions for Seismic Design of New Buildings and Other Structures, FEMA P-695*, Federal Emergency Management Agency Washington, D.C (2009).
5. Judd, J. and Charney, F. "Earthquake risk analysis of structures in structural dynamics", *EURODYN 2014*, A. Cunha, et al., Editors, Porto, Portugal, pp. 2929-2938 (2014).
6. Baker, J.W. "Quantitative classification of near-fault ground motions using wavelet analysis", *Bulletin of the Seismological Society of America*, **97**(5), pp. 1486-1501 (2007).
7. Baker, J.W. and Cornell, C.A. "Vector-valued intensity measures for pulse-like near-fault ground motions", *Engineering Structures*, **30**(4), pp. 1048-1057 (2008).
8. Tehranizadeh, M. and Shanehsazzadeh, H. "Near-fault amplification factor by using wavelet method", *Research, Development and Practice in Structural Engineering and Construction* (2011). DOI: 10.3850/978-981-08-7920-4_St-35-0117
9. Tehranizadeh, M. and Shanehsazzadeh, H. "Directivity effects on near fault amplification factor", *Urban Earthquake Engineering*, Sharif university (April 2011).
10. Yousefi, M. and Taghikhany, T. "Incorporation of directivity effect in probabilistic seismic hazard analysis and disaggregation of Tabriz city", *Natural Hazards* (2014). DOI 10.1007/s11069-014-1096-5
11. Shahi, S.K. and Baker, J.W. "An efficient algorithm to identify strong velocity pulses in multi-component ground motions", *Bulletin of the Seismological Society of America*, **104**(5), pp. 2456-2466 (2014).

12. Haselton, C.B., Liel, A., Deierlein, G.G., Dean, B.S., and Chou, J.H. "Seismic collapse safety of reinforced concrete buildings. I: Assessment of ductile moment frames", *Journal of Structural Engineering*, **137**(4), pp. 481-491 (2010).

13. Liel, A., Haselton, C.B., and Deierlein, G. "Seismic collapse safety of reinforced concrete buildings. II: Comparative assessment of nonductile and ductile moment frames", *Journal of Structural Engineering*, **137**(4), pp. 492-502 (2010).

14. Champion, C. and Liel, A. "The effect of near-fault directivity on building seismic collapse risk", *Earthquake Engineering & Structural Dynamics*, **41**(10), pp. 1391-1409 (2012).

15. Champion, C. and Liel, A. "The effect of near-fault directivity on building seismic collapse risk", Final Report to U.S. Geological Survey (Feb. 2010-Jan. 2012).

16. Haselton, C.B., Liel, A., Lange, S., and Deierlein, G. "Beam-column element model calibrated for predicting flexural response leading to global collapse of RC frame buildings", PEER Report (2007).

17. Baltzopoulos, G., Vamvatsikos, D., and Iervolino, I. "Analytical modelling of near-source pulse-like seismic demand for multi-linear backbone oscillators", *Earthquake Engng Struct. Dyn*, Published online in Wiley Online Library (wileyonlinelibrary.com) (2016). DOI: 10.1002/eqe.2729

18. Moshref, A., Tehranizadeh, M., and Khanmohammadi, M. "Investigation of the reliability of nonlinear modeling approaches to capture the residual displacements of RC columns under seismic loading", *Bulletin of Earthquake Engineering*, **13**(8), pp. 2327-2345 (August 2015).

19. Baltzopoulos, G. "Structural performance evaluation in near-source conditions", Doctorate Programme in Seismic Risk, XXVII cycle, Universit degliStudi di Napoli Federico II, Naples, Italy, http://wpage. unina.it/iuniervo/doc_en/Students.html (2015).

20. "Iranian code of practice for seismic resistant design of buildings", Standard No. 2800, 4th edition (2014).

Biographies

Homa Shanehsazzadeh is a PhD degree candidate in the Department of Civil and Environmental Engineering at Amirkabir University of Technology (Tehran Polytechnic), Tehran, Iran, where she also received her MSc degree in Earthquake Engineering in 2011. She received her BSc degree in Structural Engineering from the Civil Engineering Department of Isfahan University of Technology, Isfahan, Iran, in 2009. Her research interests include effective parameters for determining near-fault design spectrum and effects of pulse period and ductility on near-fault collapse risk.

Mohsen Tehranizadeh, PhD, is Full Professor in the Department of Civil and Environmental Engineering at Amirkabir University of Technology (Tehran Polytechnic), Tehran, Iran. He received a BSc degree in Structural Engineering from the Department of Civil and Environmental Engineering at Sharif University of Technology, Tehran, Iran. He received MSc and PhD degrees in Structural Engineering from University of California, USA, in 1977 and 1985, respectively. His research interests include application of seismic linear and nonlinear structural analysis and response to the analysis and design of seismic-resistant structures and rehabilitation of existing buildings as well as near-fault features including directivity and polarization effect, fault-fling, etc.